PAPER

Check for updates

Pore formation induced by nanoparticles binding to a lipid membrane†

Yui Tik Pang, ‡[a] Zhenpeng Ge,‡[a] Bokai Zhang,[a] Peng Xiu,[b] Quan Li[a] and Yi Wang *[a]

Nanoparticles (NPs) enter a cell primarily *via* endocytosis, during which they are engulfed by the cell and reside in lipid vesicles named endosomes. Apart from when an endosome is pinched off the plasma membrane, structural integrity of its lipid membrane is usually well maintained. Under certain circumstances, however, such structural integrity can be considerably perturbed by a nanoparticle. For instance, recent experiments [Chu *et al.*, *Sci. Rep.*, 2014, **4**, 4495] indicate that nanodiamonds with sharp corners can escape from an endosome by piercing its lipid membrane. Nonetheless, the energetics of this behavior and how it may be controlled by membrane adhesion and NP morphology remain unclear. In this work, we employ continuum modeling to investigate membrane pore formation induced by the spontaneous binding of a sharp nanoparticle. Based on two axial-symmetric NP models, we characterize the indispensable role played by curvature heterogeneity, membrane adhesion, and the sharpness as well as the size of a nanoparticle in 'breaking' a lipid membrane. Apart from revealing a general mechanism of NP binding-induced membrane pore formation, our results provide the reference for improving the endosomal escape of nanoparticles through manipulating their morphology, a direction that can be explored either independently or combined with existing strategies targeting NP surface chemistry.

Introduction

Due to the rapid development of nanotechnology, consumer products containing nanomaterials have increased rapidly over the past couple of decades.[1] In all living organisms, the plasma membrane represents the first barrier against the entry of a nanoparticle (NP) into a cell. NPs cross this barrier primarily through endocytosis, a process during which they are engulfed by the cell and reside in lipid vesicles named endosomes.[2] The specific endocytosis pathway taken by a nanoparticle, be it phagocytosis, pinocytosis, caveolae-dependent or clathrin-mediated endocytosis, depends strongly on both NP properties and cell types under investigation, reflecting the complexity of the NP endocytosis mechanism.[1,3] Following endocytosis, nanoparticles may escape from the endosome and enter the cytosol, which is particularly relevant for NPs intended as intracellular sensors or delivery vessels. Indeed, successful endosomal escape is key to improving the bio-

availability of drugs delivered by NP carriers—if these molecules remain trapped within an endosome, their therapeutic effects may be completely diminished.[4–7]

A number of strategies have been developed to engineer nanoparticles' endosomal escape.[4–7] For instance, pH-buffering agents have been exploited to create a 'proton sponge effect' to trigger endosomal swelling and lysis, thereby, releasing its contents.[4] In addition, endosomal escape can be achieved by breaking the lipid membrane. For instance, cationic gold NPs have been shown to disrupt bilayer structures[8] and cause the release of fluorescent dyes from a vesicle.[9,10] Specific modifications of the NP surface may damage the endosomal membrane *via* chemical reactions.[11] More recently, nanodiamonds (NDs) with sharp corners have been shown to pierce the endosomal membrane, thereby, escaping from the endosome vesicle.[12,13] Interestingly, such a behavior appears to be morphology dependent: NDs with a thin (~2 nm) SiO_2 coating can still make the escape, but when a thick (~15 nm) SiO_2 coating 'rounds off' their corners, NDs remain stable in the endosome.[12]

Computationally, the interactions between nanoparticles and membranes have been extensively studied *via* all-atom molecular dynamics (MD) simulations,[8,14–17] coarse-grained (CG) MD simulations,[18–24] dissipative particle dynamics (DPD) simulations[25–29] and continuum modeling.[30,31] The advantage of all-atom MD lies in its high spatial and temporal resol-

*[a] Department of Physics, Chinese University of Hong Kong, Shatin, N.T., Hong Kong.
E-mail: yiwang@cuhk.edu.hk*
[b] Department of Engineering Mechanics, Zhejiang University, Hangzhou 310027, China
† Electronic supplementary information (ESI) available. See DOI: 10.1039/C9NR10534D
‡ These authors contributed equally to this work.

utions, although the substantial computational cost often limits its application. CG MD[32,33] and DPD simulations,[34,35] which greatly extend the length and time scales of all-atom MD, have therefore become increasingly popular.[36–39] Continuum modeling based on elastic theory may be considered an extreme case of 'coarse graining' and has been applied in numerous studies of NP–membrane interactions.[40–46] Despite these extensive computational studies, however, the mechanism by which the aforementioned nanodiamonds pierce the endosomal membrane is yet to be determined. In general, while continuum modeling studies routinely examine the conditions under which NPs can, for instance, become engulfed by a lipid vesicle, they rarely treat the 'breaking' of the latter by the former. MD simulations investigating such NP binding-induced loss of membrane structural integrity are limited to small nanoparticles, while the corresponding DPD simulations often employ an external driving force or assume a strong NP–membrane adhesion. These latter conditions either do not match the spontaneous nature of nanodiamond-induced membrane disruption, or, result in a bilayer being wrapped seamlessly around an entire nanoparticle, which differs significantly from nanodiamond-containing vesicles reported experimentally.[12,13]

In this work, we employ continuum modeling to determine the energetics of nanoparticle-induced pore formation in an infinite, flat membrane. Inspired by the experimental observations on nanodiamonds,[12,13] we create two axial-symmetric models, a prolate spheroid and a rounded cone, and characterize their required geometry and membrane adhesion strength to induce pore formation. The results from the former model inform us of the critical role of curvature heterogeneity: when a prolate spheroid reduces to a sphere, pore formation becomes energetically unfavorable regardless of its size or adhesion strength. The results from the latter model, which provides finer control over its local geometry, further reveal key requirements on the NP size and sharpness to induce membrane pore formation, i.e., a nanoparticle needs to be both sharp and large enough in order to spontaneously pierce a membrane. Overall, our results not only agree well with the aforementioned experiments, but also provide a mechanistic understanding of the novel phenomenon of morphology-dependent, NP binding-induced membrane pore formation. Previous strategies for enhancing endosomal escape,[4–7] such as coating a NP with cationic polymers or cell-penetrating peptides, frequently focus on its surface chemical properties. For this reason, our findings on the morphological requirements of NP-induced pore formation may be exploited as an independent degree of freedom to enhance the endosomal escape of nanoparticles.

Methods

The systems studied in our work consist of nanoparticles interacting with an infinite, flat membrane. Our theoretical and numerical approach largely follows that of Deserno,[40] with a major difference being our explicit treatment of the possibility of a sharp NP 'piercing' the membrane. This is done by including a pore formation contribution into the total deformation energy of the membrane. Particularly, for a given nanoparticle, we first consider a membrane wrapping the NP without pore formation. This process has been well understood to be a competition between the favorable NP-lipid adhesion and the unfavorable membrane bending and stretching energy. A significant contribution to the latter comes from wrapping a highly curved region of a nanoparticle, e.g., its tip. Therefore, we next consider the energetic cost of piercing the membrane, beginning from the most curved region of the NP—a pore formed in this region lowers the bending and stretching energy of the membrane at the cost of introducing an open edge. When the released energy is greater than the edge energy, pore formation may become energetically favorable. In general, we identify the final state with the lowest energy through a two-dimensional scan over the wrapping and pore extent for a given nanoparticle. In the following, we briefly introduce the theoretical background of our calculation and the NP models considered in this work. We then discuss the shape equations for the free part of the membrane and the corresponding energetic consideration of pore formation.

Theoretical backdrop

We assume that the binding of a given nanoparticle to a membrane is driven by an adhesion energy proportional to their contact area A_{ad}:

$$E_{ad} = -\omega A_{ad} \qquad (1)$$

where ω is the adhesion constant. As reviewed by Contini et al.,[48] ω typically falls into the range of ~0.2 to $1.2 k_B T$ per nm^2, with the exception of the adhesion strength of DMPC lipid bilayers on gold electrodes measured at ~$9.7 k_B T$ per nm^2. Here, we scan a range of ω from 0.05 to $4 k_B T$ per nm^2, and adopt a representative value of $0.5 k_B T$ per nm^2 in calculations with a constant ω.

Following the classical Canham–Helfrich continuum model,[49,50] we treat the membrane as an infinitely thin elastic sheet with its bending energy (E_{bend}) in the following form:

$$E_{bend} = \int \left[\frac{k_c}{2}(2H - c_0)^2 + k_g K \right] dA, \qquad (2)$$

where k_c and k_g are the bending rigidities associated with the mean (H) and Gaussian (K) curvature of the membrane surface, respectively. Their representative values reported experimentally are adopted in this work, namely, $k_c = 20 k_B T$[51–53] and $k_g = -16 k_B T$ (see ref. 54 and references therein). Assuming a symmetric membrane, we set the spontaneous curvature c_0 to zero. By the Gauss–Bonnet theorem, $\int K dA$ is a topological invariant. Therefore, the contribution of the Gaussian curvature term to E_{bend} can be ignored as long as no pore is formed in the membrane. Apart from E_{bend}, deformation of the membrane is also penalized by a tension energy (E_{ten}). Assuming that the membrane is being pulled against a prescribed lateral tension σ, E_{ten} is proportional to A_{ex}, the
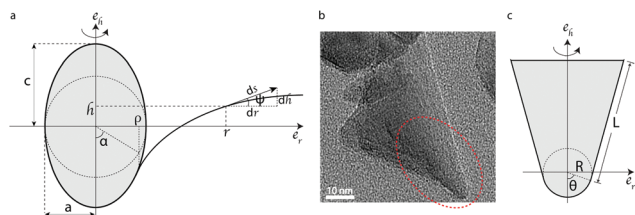
Fig. 1 Nanoparticle models considered in this work. (a) A prolate spheroid NP model with the arc-length parameterization of the membrane illustrated. (b) Representative transmission electron microscopy image of a nanodiamond studied in ref. 12 and 13. (c) A rounded cone NP model designed to mimic the tip of the nanodiamond in (b).

excess, stretched area of the membrane: $E_{ten} = \sigma A_{ex}$. With the arc-length parameterization adopted in ref. 40 and shown in Fig. 1a, E_{ten} takes the following form:

$$E_{ten} = \int \sigma (1 - \cos \psi) dA, \tag{3}$$

where ψ is the angle between the membrane arc and the horizontal. Typical cellular tension is reported to be around 0.05 mN m^{-1},[55] although it can vary from nearly zero to approximately 1 mN m^{-1} under different conditions.[56–58] In this work, apart from the representative 0.05 mN m^{-1}, we also perform our calculations at three other tension values, $\sigma = $ 0.003, 0.5, and 1.0 mN m^{-1}. These four values of σ altogether cover the range of low, medium as well as high tension regimes. Finally, we consider the possibility for pore formation within the membrane. As we assume axial symmetry in our calculations, the 'shape' of the pore is restricted to a circle and the corresponding energy cost E_{pore} is:[59,60]

$$E_{pore} = 2\pi r_p \eta, \tag{4}$$

where r_p is the pore radius and η is the line tension arising from rearranging lipid molecules at the edge of the pore. The typical value of $\eta = 10$ pN (ref. 61 and 62) is adopted in our calculation. Note that eqn (4) only corresponds to the edge energy associated with pore formation, while the mechanical work of pore expansion arising from the release of membrane tension energy is considered separately.

Summing up the above contributions gives the total energy of the NP–membrane system:

$$E_{tot} = E_{ad} + E_{bend} + E_{ten} + E_{pore}. \tag{5}$$

The calculation of E_{tot} is then divided into two parts, namely, the part of the membrane attached to the NP surface and the free part. While the former is straightforward to obtain since the shape of the membrane follows exactly that of the nanoparticle, calculation of the latter is achieved by invoking the Euler–Lagrange equation and numerically solving the resulting set of non-linear differential equations.

Model construction

Prolate spheroid. The first model considered in our work is a prolate spheroid (Fig. 1a) designed to represent the entire nanoparticle under investigation. In spherical coordinates, such a prolate spheroid is represented by $x = a \sin \vartheta \cos \phi$, $y = a \sin \vartheta \sin \phi$ and $z = -c \cos \vartheta$, where c and a are its semi-major and semi-minor axis, respectively. Note that we have defined ϑ as the polar angle with respect to the negative z axis, as it provides a convenient description of the NP-induced pore formation. To mimic the size of the nanoparticles studied in ref. 12 and 13, we first fix c to be 50 nm and scan the aspect ratio $e = c/a$ and then repeat the calculations at two additional values of c at 25 and 100 nm respectively. An additional calculation is performed with the aspect ratio e set to 7.5 while c is varied between 15 and 150 nm.

The area element of the prolate spheroid is $dA = 2\pi a \sin \vartheta \sqrt{a^2 \cos^2 \vartheta + c^2 \sin^2 \vartheta} d\vartheta$, and its mean and Gaussian curvatures are $H = c[2a^2 + (c^2 - a^2)\sin^2 \vartheta]/[2a(a^2 + (c^2 - a^2)\sin^2 \vartheta)^{\frac{3}{2}}]$ and $K = c^2/[a^2 + (c^2 - a^2) \sin^2 \vartheta]^2$, respectively. If the above NP model approaches an infinite flat membrane from above and gradually becomes wrapped at its south pole, the energy of the part of the membrane wrapping the prolate spheroid is:

$$E_{PS} = \int_0^\alpha \left[\overbrace{-\omega}^{E_{ad}} + \overbrace{2k_c H^2}^{E_{bend}} + \overbrace{\sigma \left(1 - \frac{a \cos \vartheta}{\sqrt{a^2 \cos^2 \vartheta + c^2 \sin^2 \vartheta}} \right)}^{E_{ten}} \right] 2\pi a \sin \vartheta \sqrt{a^2 \cos^2 \vartheta + c^2 \sin^2 \vartheta} d\vartheta, \tag{6}$$

where α denotes the polar angle of the location where the membrane first leaves the surface of the spheroid. Finally, a pore that forms at its south pole with a polar angle β ($0 < \beta < \pi/2$) has the energy $E_{pore} = 2\pi a \sin \beta \eta$.

Rounded cone. In the prolate spheroid model described above, sharpness is controlled by the aspect ratio, the latter of which is a global property, i.e., varying e affects the overall shape of the spheroid. To gain a finer control over the local geometric properties of our NP model, we constructed a rounded cone, the tip of which has radius R and the side of which is of length L. This model bears close resemblance to the tip part (circled region in Fig. 1b) of a nanodiamond studied experimentally. Its three geometric parameters (R, L and the angle θ shown in Fig. 1c) allow us to better separate the size of the model from its sharpness, the former of which is dictated by L while the latter is primarily set by R.

Again assuming that the above NP model approaches an infinite flat membrane from above, we obtain the energy of the membrane wrapping the tip of the rounded cone:

$$E_{RCtip} = \int_0^\alpha \left[\overbrace{-\omega}^{E_{ad}} + \overbrace{\frac{2k_c}{R^2}}^{E_{bend}} + \overbrace{\sigma(1 - \cos \vartheta)}^{E_{ten}} \right] 2\pi R^2 \sin \vartheta d\vartheta$$
$$= (4\pi k_c - 2\pi \omega R^2)(1 - \cos \alpha) + \sigma \pi R^2 (1 - \cos \alpha)^2, \tag{7}$$

where α again denotes the location where the membrane first leaves the surface of the tip ($0 \leq \alpha \leq \theta$).

If the membrane continues to wrap the side of the rounded cone, it becomes more convenient to switch to the cylindrical coordinate. Temporarily shifting the origin to the vertex of the cone, one obtains its representation as $x = \dfrac{u}{\tan \theta} \cos \phi$, $y = \dfrac{u}{\tan \theta} \sin \phi$ and $z = u$. The area element is $dA = \dfrac{2\pi u}{\tan \theta \sin \theta} du$, while the mean curvature is $H = \dfrac{\tan \theta \sin \theta}{2u}$ and the Gaussian curvature $K = 0$. The corresponding energy of the membrane is therefore:

$$E_{RCside} =$$

$$\int_{R \tan \theta \sin \theta}^{(R \tan \theta + L') \sin \theta} \left[\overbrace{-\omega}^{E_{ad}} + \overbrace{2k_c \left(\frac{\tan \theta \sin \theta}{2u} \right)^2}^{E_{bend}} + \overbrace{\sigma(1 - \cos \theta)}^{E_{ten}} \right] \frac{2\pi u}{\tan \theta \sin \theta} du$$

$$= (2\pi R L' \sin \theta + \pi L'^2 \cos \theta)[\sigma(1 - \cos \theta) - \omega]$$

$$+ k_c \pi \frac{\sin^2 \theta}{\cos \theta} \ln \left(1 + \frac{L'}{R \tan \theta} \right),$$

(8)

where L' denotes the length of the side of the cone wrapped by the membrane ($0 \leq L' \leq L$). It should be noted that we do not consider membrane wrapping beyond the side of the rounded cone, i.e., the membrane does not curve back to wrap the base of the cone. Energetically such wrapping is prohibited by the infinite curvature along the rim of the base, i.e., where the generatrix meets the directrix of the cone. Practically it is also of little relevance, since the rounded cone model mimics only the tip part of a nanodiamond. Along this line, we also restrict θ to the range $\left(0, \dfrac{\pi}{2} \right)$ in our calculation, since a model with $\theta \geq \dfrac{\pi}{2}$ loses resemblance to the NPs studied experimentally. Finally, if a pore with polar angle β forms at the spherical tip of the rounded cone NP, its energy is simply $E_{pore} = 2\pi R \sin \beta \eta$. If it continues to grow and spans a length L_p along the side of the cone, its energy becomes $E_{pore} = 2\pi \eta (R \sin \theta + L_p \cos \theta)$.

Shape equation of the free part of the membrane

The energy of the free part of the membrane (E_{free}) only consists of two contributions: bending and stretching. Following ref. 40, we obtain its two principle curvatures as $\dfrac{\sin \psi}{r}$ and $\dot{\psi}$, where the superscript dot represents a derivative with respect to the arc length s. A Lagrange function $\mathcal{L}$ can then be setup:[63]

$$\mathcal{L} = r \left[\left(\dot{\psi} + \frac{\sin \psi}{r} \right)^2 + \frac{2\sigma}{k_c} (1 - \cos \psi) \right]$$
$$+ \lambda_r (\dot{r} - \cos \psi) + \lambda_h (\dot{h} - \sin \psi),$$

(9)

where the first two terms in the bracket represent the bending and tension energy, respectively, while the last two terms enforce the constraints $\dot{r} = \cos \psi$ and $\dot{h} = \sin \psi$.[40] Finally, E_{free} is given by $E_{free} = \pi k_c \int_0^\infty \mathcal{L} ds$. Switching to the

Hamiltonian description we obtain the full set of shape equations, which are presented in the ESI,† along with their boundary conditions. The numerical solution of these shape equations is found through a shooting algorithm where the only missing boundary condition at the membrane–NP contact point, namely, $\dot{\psi}(0)$, is scanned to achieve asymptotic flatness of the membrane.[40] The resulting E_{free} is then added to E_{PS} or E_{RCtip} and E_{RCside} to yield E_{tot}. This calculation is first performed for a given wrapping degree of an NP model without considering pore formation, and is then followed by a scan over the pore size as described below.

Pore formation energetics. Unlike in a free membrane, pore formation energetics in a membrane attached to a nanoparticle concerns not only the straightforward E_{pore} term. First, the area on the NP surface exposed upon pore formation releases certain adhesion, bending and stretching energy. These terms are readily evaluated with eqn (6) to (8). Second, since pore formation signals topological change of the membrane, the previously ignored Gaussian curvature contribution to E_{bend} must now be considered. Invoking the Gauss–Bonnet theorem, $\int^K dA$ over the free part of the membrane can be calculated from integrating the geodesic curvature around the pore edge. Equivalently, it may also be obtained by negating over the area initially covered by the membrane before pore formation. For instance, assuming that a pore forms at the south pole of the prolate spheroid with a polar angle β, the Gaussian curvature contribution to the bending energy is now $E_{gau} = -2\pi k_g \left(1 - a \cos \beta / \sqrt{a^2 \cos^2 \beta + c^2 \sin^2 \beta} \right)$. Similarly, in the rounded cone model, if the pore forms only within the spherical tip, the resulting E_{gau} is $-2\pi k_g (1 - \cos \beta)$. Once the pore covers the entire spherical tip, $E_{gau} = -2\pi k_g (1 - \cos \theta)$. As the Gaussian curvature is everywhere zero on the cone surface, further growth of the pore onto the side of the cone does not change E_{gau}. Finally, summing up E_{pore}, E_{gau} and the released energy due to the receding of the membrane, we obtain ΔE_{tot}, the change in E_{tot} upon pore formation. For a given wrapping extent ρ, defined as the radial coordinate of the location where the membrane leaves the NP surface (Fig. 1a), we vary the pore size from zero to ρ and record the corresponding new E_{tot}. Through this two-dimensional scan, we identify the final state of the NP–membrane system with the minimum energy.

It is worth noting that in the above calculations the pore never grows onto the free part of the membrane, i.e., the membrane always remains attached to the surface of our NP models. As a result, the shape of the free part of the membrane is unaffected by the presence of the pore, which is fundamentally different from a membrane with a free open edge.[64,65] The latter scenario is not considered here as under such a condition, no NP–membrane adhesion is retained and the resulting E_{tot} is inevitably positive. The nanoparticles would therefore stay detached from the membrane ($E_{tot} = 0$).

Results

Prolate spheroid NP

Spherical NP. Before we discuss the results of prolate spheroids, it is instructive to consider first a spherical nanoparticle, which may be interpreted as a special prolate spheroid with an aspect ratio of 1. The energy of the part of the membrane attached to this NP can be readily obtained either by setting $a = c = R$ in eqn (6) or simply by invoking eqn (7): $E_{sphere} = E_{RCtip}$. Note that in the latter case the rounded cone is assumed to contain only its tip ($\theta = \pi$). The energy of the free part of the membrane is non-negative—at $\sigma = 0$ it adopts the shape of catenoids,[40] which leads to $E_{free} = 0$; otherwise, $E_{free} > 0$. The total energy of the NP–membrane system is therefore $E_{tot} = E_{sphere} + E_{free} \geq E_{sphere}$.

If we now assume that a pore with a polar angle β forms at the south pole of this spherical NP, the change in E_{tot} is

$$\Delta E_{tot} = -\overbrace{\left\{ (4\pi k_c - 2\pi\omega R^2)(1-\cos\beta) + \sigma\pi R^2(1-\cos\beta)^2 \right\}}^{\text{released part of } E_{sphere}}$$
$$+\underbrace{2\pi R \sin\beta\eta}_{E_{pore}} \underbrace{-2\pi k_g(1-\cos\beta)}_{E_{gau}}. \tag{10}$$

Despite the seemingly complex form of ΔE_{tot}, it renders the discussion of pore formation in spherical NPs rather straightforward: clearly, its last two terms (E_{pore} and E_{gau}) are both non-negative. Therefore, if pore formation is to be more favorable than the pore-free state, its first term must be negative, which immediately leads to the condition $\omega < \frac{2k_c}{R^2} + \frac{\sigma}{2}(1-\cos\beta)$. Meanwhile, if pore formation is to be more favorable than the detached/free state, the energy associated with the remaining part of the membrane attached to the NP surface, which is simply the sum of E_{sphere} and the first term in eqn (10), must be negative. This requirement leads to $\omega > \frac{2k_c}{R^2} + \frac{\sigma}{2}(1-\cos\beta) + \frac{\sigma}{2}(1-\cos\alpha)$, which clearly contradicts the previously derived condition.

Therefore, regardless of its size, pore formation is always energetically unfavorable for a spherical NP. This result can be qualitatively explained by the homogeneity of a spherical surface—pore formation only becomes favorable when the energy released from a highly curved region outweighs the cost of introducing an open edge, while the remaining, less curved regions should maintain membrane adhesion to yield a negative E_{tot}. Since no part of a spherical surface is more or less curved than other parts, a spherical NP can never induce energetically favorable pore formation by itself. As found previously,[40] when its curvature becomes very large, the membrane simply stays detached from the NP.

Prolate spheroid NP. The phase diagram of a prolate spheroid NP with $c = 50$ nm and an aspect ratio e ranging from 2 to 20 is shown in Fig. 2a. At a low aspect ratio, e.g., $e = 3$, no pore formation occurs, while the state with the lowest energy changes from free to partial wrapping and then to complete
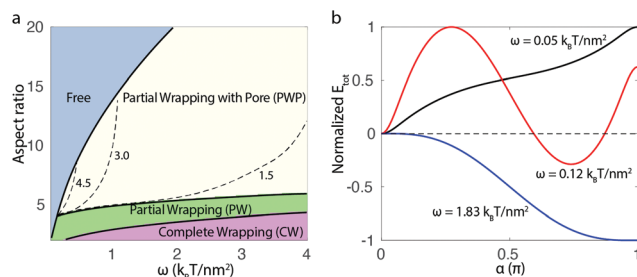

Fig. 2 Phase diagram (a) and normalized total energy (b) of a membrane wrapping a prolate spheroid NP with $c = 50$ nm at $\sigma = 0.05$ mN m^{-1}. Dashed curves in (a) represent contour lines of pore radius (unit: nm). The plots of normalized E_{tot} as a function of wrapping degree α shown in (b) are obtained with $e = 3.5$ and correspond to the free (black), partial wrapping (red) and complete wrapping (blue) state, respectively.

wrapping as the adhesion strength ω increases (Fig. 2b). This behavior is similar to membrane wrapping of a spherical colloid.[40] Such a similarity is to be expected, since at a low aspect ratio the prolate spheroid largely resembles a sphere. One difference, however, is that unlike a spherical NP, the transition from the free to partial wrapping state is discontinuous, with an energy barrier arising from wrapping the highly curved tip of the prolate spheroid (Fig. 2b).

Once e increases to beyond 4.1, pore formation becomes accessible. With the semi-major axis of the prolate spheroid fixed at $c = 50$ nm, this corresponds to a semi-minor axis of $a \approx 12$ nm. A prolate spheroid NP this 'sharp' can induce pore formation when the adhesion strength is above a certain threshold. As its aspect ratio increases, the required threshold value also increases, as indicated by the boundary separating the free and the PWP state shown in Fig. 2a. With e reaching beyond 4.4, the complete wrapping state is no longer accessible within the range of ω examined here. Further increase in the aspect ratio to beyond ~6 also squeezes out the pore-free partial wrapping state.

For a given aspect ratio, the largest pore is achieved at an intermediate adhesion strength. For instance, with $e = 6$, the pore radius is approximately 5.0 nm with $\omega = 0.3k_BT$ per nm^2 and decreases to approximately 3.0 nm with $\omega = 0.7k_BT$ per nm^2. This result reflects the competition between membrane wrapping and pore formation: if ω is too strong, only a small pore can be afforded due to the highly favorable NP–membrane adhesion; meanwhile, if the adhesion strength is too weak, neither of the above two states is favorable and the membrane stays detached from the prolate spheroid.

The above calculations were performed at the membrane tension of $\sigma = 0.05$ mN m^{-1}. Decreasing σ to 0.003 mN m^{-1} reduces the energetic cost of wrapping and pore formation, effectively shifting the phase diagram horizontally to the left, where pore formation can be achieved at a smaller ω (Fig. S1a†). Conversely, increasing σ to 0.5 mN m^{-1} and 1.0 mN m^{-1} gradually shifts the phase diagram to the right, favoring the free state instead (Fig. S1b and c†). As shown in

Fig. S2a and b,† a decrease in c shifts the phase diagram towards the lower right, whereas an increase in c has the opposite effect. At a given aspect ratio and adhesion strength, Fig. S2c† indicates that larger particles are more likely to be wrapped by the membrane, a well-known result from previous studies.[40,43] Notably, the PWP state, which only becomes favorable when c is large enough, will become inaccessible again as c further increases, i.e., a prolate spheroid at a given e needs to be neither too small nor too large in order for pore formation to be energetically favorable.

Rounded cone NP

The results from the previous section indicate that a 'sharp enough' prolate spheroid is capable of inducing membrane pore formation. However, the resemblance between a prolate spheroid and a nanoparticle examined experimentally[12] (Fig. 1b) is clearly limited. In addition, sharpness cannot be controlled locally in a prolate spheroid, since varying the aspect ratio alters curvatures over its entire surface. With c kept a constant, a change in the aspect ratio also affects the size of the prolate spheroid along the semi-minor axis. In order to overcome these limitations, we constructed a rounded cone to represent the tip of the nanoparticle studied experimentally (Fig. 1). This model allows fine control over its geometric properties: its size is predominantly determined by the

edge length L, and the sharpness at its tip is determined by the radius R. The angle θ controls the 'tilting' of the edge, which, in turn, affects the mean curvature on the cone surface.

Wrapping energetics. The energetics of a membrane wrapping the rounded cone NP consists of two parts: wrapping the spherical tip and wrapping the side of the cone. A close look at the energy of the latter part (eqn (8)) reveals that when adhesion is extremely weak ($\omega < \omega_{min}$, where $\omega_{min} \equiv \sigma(1 - \cos\theta)$), E_{RCside} is positive, i.e., wrapping the side of the cone is unfavorable regardless of the length of the wrapped part (L'). Under this condition and given the set of parameters studied in this work, it turns out that wrapping of the spherical tip is also unfavorable, i.e., $E_{RCtip} > 0$. Therefore, the membrane prefers to stay detached from the entire nanoparticle under such a weak adhesion.

It should be emphasized that ω_{min} is not the minimum ω required to achieve wrapping for a given rounded cone, which corresponds to the boundary separating the free state from other states in the phase diagram shown in Fig. 3b and cannot be expressed in an analytic form. The significance of ω_{min} is rather the following: with $\omega > \omega_{min}$, for any given tip radius R and tilt angle θ, complete wrapping of the rounded cone NP can be achieved with a large enough L. This result is further illustrated in Fig. 3a and 4a, and is explained by the form of E_{RCside}—at large L', E_{RCside} is dominated by the adhesion term,
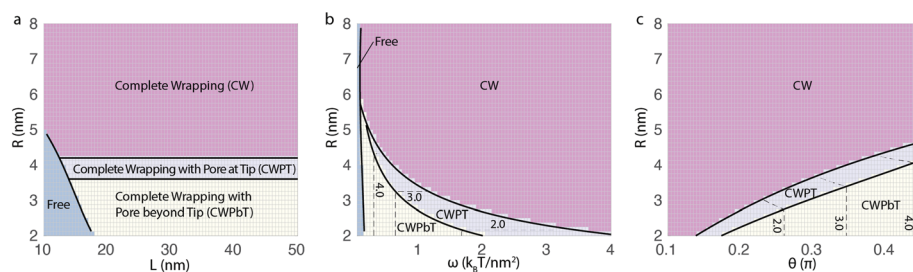

Fig. 3 Phase diagrams of the rounded cone NP at $\sigma = 0.05$ mN m^{-1} with (a) $\theta = 0.375\pi$ and $\omega = 0.5k_BT$ per nm^2, (b) $\theta = 0.375\pi$ and $L = 50$ nm, (c) $L = 50$ nm and $\omega = 0.5k_BT$ per nm^2. Dashed curves represent contour lines of pore radius (unit: nm). In CW, CWPT and CWPbT states, the membrane wraps the entire surface of the rounded cone (excluding its base), with either no pore (CW), a pore forming at its tip (CWPT) or a pore growing beyond the tip onto the side of the rounded cone (CWPbT).
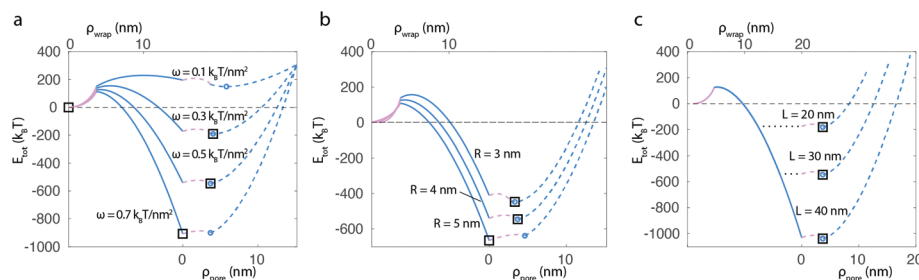

Fig. 4 One-dimensional energy profiles of E_{tot} as a function of the wrapping and pore extent at $\sigma = 0.05$ mN m^{-1} with (a) $\theta = 0.375\pi$, $R = 4.0$ nm and $L = 30$ nm, (b) $\omega = 0.5k_BT$ per nm^2, $\theta = 0.375\pi$, and $L = 30$ nm, (c) $\omega = 0.5k_BT$ per nm^2, $\theta = 0.375\pi$, and $R = 4.0$ nm. Membrane wrapping of the tip and the side of the rounded cone is shown as solid red and blue curves, while pore formation at these two parts are shown as dashed red and blue curves, respectively. Black squares indicate the locations with the minimum E_{tot}, while blue circles represent the locations with the minimum ΔE_{tot} once a pore grows onto the side of the rounded cone. As described in the Methods section, the wrapping and pore extent ρ is defined as the radial coordinate of the location where the membrane leaves the NP surface or forms a pore. For clarity, the wrapping extent (ρ_{wrap}) and pore extent (ρ_{pore}) are labeled in the upper and lower x-axis, respectively.

which scales quadratically as the wrapped edge length L'. Therefore, as long as ω exceeds the aforementioned threshold, it is always possible to increase L, and, correspondingly, L', to render E_{RCside} negative enough. Note that even with the maximum $\sigma = 1.0$ mN m^{-1} and $\theta = 0.45\pi$ considered in our calculations, the value of ω_{min} is only $\sim 0.2 k_B T$ per nm^2, which coincides with the lower boundary of typical adhesion strength reported in the literature.[48]

Further analysis of E_{RCside} reveals that under the condition $\omega > \omega_{min}$, E_{RCside} achieves a maximum at $L_{E_{max}} = \tan \theta \left(\sqrt{k_c/2[\omega - \sigma(1 - \cos \theta)]} - R \right)$. Temporarily putting aside the contribution of E_{free}, we can attempt an approximate analysis of the membrane wrapping behavior along the side of the rounded cone: if $L_{E_{max}} < 0$, it is immediately clear that complete wrapping is always favorable; if $L_{E_{max}} > 0$, wrapping of the side of the cone can become unfavorable when the edge length L is not large enough and the membrane attaches, if at all, to the tip of the rounded cone only. This latter scenario, however, is of little interest here, since it reduces to the spherical NP case examined earlier, where it has been shown that pore formation is never favorable for a spherical nanoparticle alone. Adding back the ignored contribution of E_{free} complicates the above analysis—the possibility of partial wrapping of the side of the rounded cone can no longer be excluded. Nonetheless, such partial wrapping is never recorded in the parameter space examined in our work. As shown in Fig. 3, the wrapping extent is either zero (membrane detached from the NP) or complete (excluding the base of the rounded cone). We should add that a different mode of partial wrapping, in which the nanoparticle tilts to touch the membrane with one side of its cone surface, becomes possible when we forgo the axial symmetry assumption in our calculations. Such axial-asymmetric modes of NP–membrane interactions are discussed briefly in the next section.

Pore formation energetics. Similar to the calculations of wrapping extent described above, we consider pore formation in our rounded cone NP a two-stage process: a pore may (1) form at the spherical tip and then (2) grow onto the side of the rounded cone. Overall, as described in the Methods section, the free part of the membrane is unaffected by the pore formation extent considered in our work. ΔE_{tot}, the change in E_{tot} relative to the pore-free state, therefore, is solely determined by the Gaussian curvature contribution E_{gau}, the released energy due to the receding of the membrane, as well as the associated E_{pore}. The analytic forms of ΔE_{tot} in the above two-stage pore formation are given in the ESI.† Based on analysis detailed therein, we conclude that for a pore limited to the spherical tip of the nanoparticle, ΔE_{tot} is a minimum at $r_p = R \sin \theta$, where r_p denotes the radius of the pore. In other words, if a pore forms at all, it covers at least the entire spherical tip of the rounded cone. The same analysis reveals that under the previously discussed condition $\omega > \omega_{min}$, a pore that grows onto the side of the rounded cone achieves a minimum ΔE_{tot} at a finite (and generally small) edge length L_p.

A close examination of the phase diagrams in Fig. 3, Fig. S3,† and the one-dimensional energy profiles in Fig. 4

reveals the relationship between the pore size and various parameters considered here: first, while a large enough L is one prerequisite for pore formation, once this condition is met, the pore size is independent of L. Second, for pores that are limited to the spherical tip, its size is also independent of ω, which can be explained by the aforementioned analysis of ΔE_{tot}: pore formation at the tip, if it happens at all, will cover the entire tip of a rounded cone. Therefore, the pore radius depends only on R and θ in a pre-defined, straightforward manner: $r_p = R \sin \theta$. Finally, when the pore grows onto the side of the cone, its radius becomes independent of R. This behavior is reflected in the expression of L_p, the only R-dependent terms of which are canceled upon the calculation of pore radius (see ESI† for details), and can also be appreciated from the following argument: once the pore grows onto the side of the cone, it no longer 'remembers' the geometry of the spherical tip. Its size therefore is solely determined by the adhesion strength and geometry of the cone, *i.e.*, the value of θ. Similar to the case of the prolate spheroid, the largest pore is obtained at an intermediate adhesion strength (Fig. 3b).

The one-dimensional (1-D) energy profiles in Fig. 4 are generated along a pseudo reaction pathway in which we monitor the system's energy as the membrane first wraps the entire rounded cone and then a pore begins to grow from its south pole. While such a pseudo reaction pathway provides a convenient 1-D analysis of membrane energetics, it may not be the actual pathway followed by the system during its transition from, for instance, the free to the CWPT or CWPbT state (Fig. 3). To identify the true transition pathway, or, the minimal energy path (MEP), we employed the string method,[66,67] which has been previously employed to capture the critical nucleus structure and energy barrier in membrane pore formation.[68] As revealed by Fig. 5 and Fig. S4,† a scan through the two-dimensional space of normalized wrapping *versus* pore extent shows that our NP-induced pore formation does not proceed in the wrapping-first-pore-second manner. Instead, the MEP corresponds to a path in which the pore grows to its equilibrium size first, followed by wrapping of the
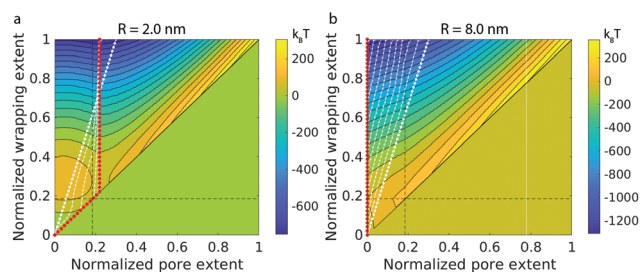

Fig. 5 Two-dimensional energy profiles of E_{tot} as a function of the normalized wrapping and pore extent at $\sigma = 0.05$ mN m^{-1}, $\omega = 0.5 k_B T$ per nm^2, $\theta = 0.295\pi$, $L = 30$ nm with (a) $R = 2.0$ nm and (b) $R = 8.0$ nm. The final MEPs determined by the string method are shown in red dots, while the initial strings are shown in big white dots, with small white dots representing the evolution of the strings. The boundary between the tip and the side of the rounded cone is marked by black dashed lines.

rest of the rounded cone. On the 1-D profiles, such a MEP amounts to bypassing part of the solid curves in Fig. 4.

The above result on MEP underscores the nature of pore formation, *i.e.*, it is an activated process with an often substantial energy barrier. For instance, with $\omega = 0.5k_BT$ per nm^2, $R = 2.0$ nm, $\theta = 0.295\pi$, and $L = 30$ nm, the barrier of pore formation induced by the rounded cone is around $86k_BT$ at the membrane tension of $\sigma = 0.05$ mN m^{-1}, much greater than the typical $40k_BT$ barrier estimated for pore formation observable experimentally.[47] It is interesting, however, to further analyze the nature of this large energy barrier. As hinted by the expression of ΔE_{tot} (see ESI†), the edge energy E_{pore} and the Gaussian curvature contribution E_{gau} are two major contributors to the energy barrier against NP-induced pore formation. The former accounts for the cost of pinching a hole in a flat membrane, whereas the latter arises from deforming the flat membrane to achieve wrapping of the nanoparticle. Within the experimentally relevant range of parameters examined in this work, these two contributions can both be significant. For instance, out of the aforementioned $86k_BT$ barrier, E_{pore} and E_{gau} each contributes $36k_BT$ and $40k_BT$, respectively. Clearly, if the E_{gau} term can be reduced, the energy barrier to NP-induced pore formation may readily fall into the range of previous estimations.[47] Such a possible scenario is further discussed in the next section.

Conditions for pore formation. As noted earlier, if a rounded cone NP is to pinch a hole in the membrane, the hole is at least as large as its spherical tip. The membrane adhesion to the side of the rounded cone thus provides the sole driving force of this process. As a result, wrapping of the side of the cone must be energetically favorable, *i.e.*, $\omega > \omega_{min}$ is one prerequisite for pore formation. There is, however, also an upper limit for ω for a given rounded cone NP (ω_{PT}), beyond which adhesion is so favorable that the cost of bending and stretching even at a highly curved tip can be well compensated. It turns out that ω_{PT}, which corresponds to the boundary separating the complete wrapping from the CWPT state in Fig. 3b, can be obtained analytically:

$$\omega_{PT} = \frac{k_g + 2k_c}{R^2} - \frac{\eta \sin\theta}{(1 - \cos\theta)R} + \frac{\sigma}{2}(1 - \cos\theta). \quad (11)$$

The derivation of ω_{PT} and ω_{PbT}, the latter of which corresponds to the boundary separating the CWPT from CWPbT state, is provided in the ESI.† Together with Fig. 3b, they allow one to estimate the range of adhesion strength over which pore formation is achievable for a given rounded cone NP. For instance, as shown in Fig. 3b, with $R = 4$ nm, increasing ω from $0.05k_BT$ per nm^2 to $0.15k_BT$ per nm^2 shifts the equilibrium state from free to CWPbT, while further increasing ω to $0.4k_BT$ per nm^2 shifts the state to CWPT. Finally, increasing ω to beyond $0.6k_BT$ per nm^2 results in complete wrapping (without pore formation) of the nanoparticle.

The above equation can be readily converted into a geometric requirement on R and θ to achieve pore formation at a given adhesion strength. For instance, with a given θ, eqn (11) becomes a quadratic equation in R, the only positive root of which corresponds to R_{PT}, the largest tip radius for which pore formation by the rounded cone NP is energetically favorable. Similarly, at fixed R, the smallest angle θ at which pore formation may occur (θ_{PT}) can again be obtained by treating eqn (11) as a root finding problem. Overall, eqn (11) provides a formula to manipulate the geometry of a rounded cone NP to enable pore formation at a given adhesion strength. An additional geometric requirement, as discussed earlier, is a large enough edge length L, which is needed to provide sufficient adhesion strength to maintain membrane–NP attachment. Unfortunately, this last requirement on L lacks an analytic form, although a cubic polynomial obtained *via* least squares fitting appears to provide a reasonably good approximation (Fig. 3 and Fig. S3†). For instance, with $R = 3$ nm, reducing L to below ~15 nm shifts the system from pore formation to the free state. Notably, the maximum pore size is also achieved along the boundary separating the CW and the CWPT states, as reflected by the contour plots of pore radius shown in Fig. 3b and c. Analysis of eqn (11) therefore enables one to maximize the pore size when, for instance, the adhesion strength is fixed at a given value. In this case, the pore size increases as θ increases, *i.e.*, as the tilt of the cone surface becomes more 'steep'. Meanwhile, the pore size also grows as R increases, although the latter must be kept below the threshold value R_{PT} mentioned above.

Discussion

The endosomal escape of nanoparticles is an important step in their intracellular delivery of cargoes ranging from DNA, short interfering RNA to proteins and small molecules.[4] If unable to escape, these cargo molecules can be degraded when the environment turns acidic as the endosome matures and eventually fuses with a lysosome. A number of strategies, including membrane fusion for liposomal NPs, osmotic rupture *via* the proton sponge effect, and membrane destabilization by synthetic polymers or peptides, have been developed to enhance nanoparticles' endosomal escape.[4–7] NP delivery vessels that combine a mesoporous silica core with a supported lipid bilayer surface, *i.e.*, protocells,[69,70] have also been developed. Through incorporating endosomolytic peptides on their surfaces *via* lipid headgroup modifications, these multifunctional NP carriers may induce endosome swelling and disruption, thereby, facilitating the release of their cargoes into the cytosol.[70] While it is generally accepted that the shape of a nanoparticle plays an important part in modulating its uptake and intracellular trafficking, a quantitative understanding of how NP morphology may be manipulated to break a lipid membrane is largely missing. Indeed, most of the endosomal escape enhancement strategies mentioned above focus on (surface) chemical rather than physical properties of a nanoparticle.

In this work, we reveal the mechanism and quantify the energetics of membrane pore formation induced by the spon-

taneous binding of a sharp nanoparticle. While our calculations were inspired by endosomal escape experiments performed with nanodiamonds, the results are general in describing NP-induced membrane pore formation. Upon reducing the prolate spheroid model to a sphere, we show that pore formation is never favorable for such a nanoparticle alone. Curvature heterogeneity, therefore, is a prerequisite for energetically favorable NP-induced pore formation: some part of the NP surface needs to be less curved than the other part, so that membrane adhesion can be retained over the former surface. Furthermore, in order to spontaneously pierce a membrane, our results indicate that a nanoparticle needs to be both sharp and large enough. An immediate question that arises is 'how sharp (large) is sharp (large) enough?' At a given adhesion strength, eqn (11) allows one to quantify the 'critical sharpness' for the rounded cone model—it provides the formula to ensure pore formation by tuning the sharpness of the nanoparticle, which is primarily controlled by the tip radius R and to a lesser degree, the tilting angle θ. Within the range of experimentally relevant parameters scanned in our calculations, a tip radius less than ∼4–5 nm is generally required (Fig. 3). This upper limit agrees well with the electron microscopy images of nanodiamonds that escape from an endosome (Fig. 1b and ref. 12). As for the question 'how large is large enough?', while no analytic expression for the required edge length L is available, numerical estimation (Fig. 3 and Fig. S3†) shows that an L of at least ∼20 nm is generally needed. This finding is again in line with the geometry of escaped nanodiamonds.[12]

Collectively, the above results provide a quantitative reference for engineering NP morphology towards improved endosomal escape. For instance, with tips that can be reasonably approximated as rounded cones, sharp corners or asperities with a radius of ∼4–5 nm may be introduced onto the surface of a nanoparticle, while ensuring that it has a long enough edge (∼20 nm). If the NP–membrane adhesion strength can be measured, a more accurate estimate of the desired morphology can be obtained using eqn (11). For layered nanocarriers such as protocells, the morphological manipulation can be performed on the core structure, although it should be noted that sharp tips added onto the silica core will be exposed to the solvent due to the large energetic cost of wrapping these highly curved parts by a supported lipid bilayer. Given the small areas they occupy, these exposed tips should not significantly alter the surface chemistry of a protocell. However, whether the loaded cargoes are still well sealed in the resulting structure will need to be verified experimentally. In general, morphological manipulation of a nanocarrier is often independent from the modification of its surface chemistry. Therefore, while the former approach is explored, the latter can be simultaneously employed to, for instance, modulate NP–membrane adhesion strength, or, introduce existing endosomolytic agents. These joint strategies may bring about further enhanced escape efficiency in the designed nanocarriers.

Most nanoparticles studied experimentally should meet the aforementioned curvature heterogeneity requirement. For spherical nanoparticles, this can be achieved by placing them on a surface, thereby, enabling energetically favorable pore formation, as has been reported by Roiter *et al.* using supported lipid bilayers.[71,72] It should be added, however, that for NPs smaller than or comparable in dimension to the bilayer thickness, the continuum model of a membrane begins to fail and needs to be replaced by a molecular description of individual lipids. Depending on their surface properties, these small nanoparticles may directly penetrate the membrane by, for instance, 'dissolving' into the hydrophobic lipid tail region,[18] or, inducing local defects through strong charge–charge interactions.[19]

Our calculations with both prolate spheroid and rounded cone models reveal a wide range of adhesion strength over which NP-induced pore formation can be favorable, *i.e.*, from a couple of tenths to a few k_BT per nm^2. This wide range of ω, which covers the typical NP–membrane adhesion strength of ∼0.2–1.2k_BT per nm^2 reported in the literature,[48] is in line with the NP escape behaviors reported by Chu *et al.*[12,13] Apart from nanodiamonds, these experiments also include gold nanoparticles and NDs with SiO_2 coating. While NPs with different surface chemistry may have a similar membrane adhesion strength, the wide range of ω over which NP-induced pore formation is achievable may also have contributed to the robust NP escaping patterns observed in these experiments.

Apart from the aforementioned endosomal escape of nanodiamonds, disruption of membrane structural integrity by NPs with sharp corners has also been reported for graphene microsheets. For instance, combining *in vitro* cell imaging with coarse-grained and atomistic simulations, Li *et al.*[28] showed that while an ideal, atomically smooth graphene sheet cannot penetrate a lipid membrane, such penetration can be readily achieved in experimentally fabricated graphene, the latter of which has rough edges. The penetration is found to be initiated by a spontaneous, localized piercing of the membrane at sharp corners or protrusions along the graphene edge. While this observation is consistent with the existence of a critical sharpness found in our calculations, more quantitative comparison between the two is prohibited by the distinction between graphene, effectively a 2-D material, and the 3-D NP models considered here. Nonetheless, our results afford quantitative and reasonably good comparison with the atomic force microscopy measurements by Roiter *et al.*[71,72] These authors systematically varied the nanoscale roughness of a mica surface by depositing on it spherical NPs with diameters ranging from 1.2 to 22 nm. They monitored the presence of pores in a DMPC supported lipid bilayer formed on the resulting surface and showed that NPs with diameters in the aforementioned range pierced the membrane, whereas larger particles were covered by intact DMPC bilayers. Assuming a 5 nm thickness of a supported lipid bilayer, the pore formed by a spherical NP with the critical radius of 11 nm has $r_p \approx 7$ nm, about 2 nm larger than the maximum pore size found in our calculations. This difference can be explained by the different geometries of the systems under investigation: a spherical NP

deposited on a flat surface has $L \to \infty$ and $\theta > \frac{\pi}{2}$. As a result of this unique geometry, the free/detached state is eliminated from the phase space; furthermore, DMPC molecules lining the pore are no longer entirely exposed to the solvent—instead, as a pore shrinks around the nanoparticle placed on mica surface, lipids along the pore rim can 'touch' the polar NP and form favorable contact—this likely lowers the line tension associated with an open edge, thus, allowing bigger pores to be formed by more blunt nanoparticles.

As described in the Methods section, we assumed axial symmetry in our calculations to simplify the derivation and numerical solution of the shape equations. If we forgo this assumption, the reaction pathways examined in our calculations become a subsection of the new, complete phase space, where the nanoparticle may freely rotate to interact with the membrane in an arbitrary orientation. For elongated NPs, Dasgupta et al.[44] found two main entry modes for their endocytosis, namely, the 'submarine' and 'rocket' modes, in which the NP long axis is either parallel or perpendicular to the membrane, respectively.[44] Depending on its morphology and membrane adhesion strength, the nanoparticle may switch between these two modes.[44] In addition, previous studies indicate that the orientation of a nanoparticle during endocytosis may also depend on the speed of its internalization.[21,23] Although the computation of axial-asymmetric NP–membrane binding modes is beyond the scope of the current work, it is tempting to conduct a qualitative analysis: take again the rounded cone as a model system, instead of its highly curved tip, the membrane can now wrap the side of the cone first, which is analogous to the submarine mode mentioned above. Similar to the results presented therein[44] and in contrast to the tip-first mode, membrane wrapping in the submarine mode is expected to be continuous (with no energy barrier). Under an intermediate adhesion strength, partial wrapping in this mode can also be expected to have the lowest energy, in which state the rounded cone 'lies down' and adheres to the membrane with its relatively flat side. The resulting membrane deformation can be rather small in such a partial wrapping state and NP-induced pore formation may therefore face a reduced energy barrier—since the membrane needs not to deform as drastically compared with the complete wrapping state, a smaller E_{gau} term can be expected. This is somewhat analogous to placing a sharp pencil horizontally on a piece of paper and then slightly deforming the paper to let the pencil tip pierce it through. Compared with seamlessly wrapping the entire pencil, deformation to the paper is minimal, so the term E_{gau}, and, therefore, the total pore formation energy barrier, may be lowered significantly. We plan to further examine these axial-asymmetric modes in our future work.

Apart from the imposed axial symmetry, a number of other caveats in our calculations should be pointed out: firstly, with the simplification of the membrane as an infinite elastic sheet, no effect of volume change, such as the potential leakage from a vesicle upon pore formation, is included. Along this line, rupture of a finite membrane when the bilayer is stretched beyond a threshold is also not considered in our work. Such stress-induced rupture, however, generally requires a large contact area, as seen in vesicle-wall adhesion.[73] Secondly, we also neglect hydrodynamic effects of the solvent, which, along with vesicle volume change, have been found to play a non-trivial role in the shape evolution of lipid vesicles near a solid surface.[47] Thirdly, our calculations are solely concerned with the energetics, rather than the dynamics, of pore formation. In our calculations a nanoparticle-induced pore can be thermodynamically stable, whereas in experiments nanodiamonds are known to entirely escape from an endosome within a few hours and the endosome vesicle is often destroyed during this process.[12] Clearly, to study such an entire escape process, a kinetic model of membrane failure[74] or the explicit consideration of pore edge propagation under the influence of vesicle volume change and solvent hydrodynamics,[47] will likely be required. Molecular details of the pore structure may also need to be taken into account in order to more accurately estimate its formation barrier.[68] Finally, how the pore formation process examined here may be affected by the presence of protein corona,[75] which can alter both the surface chemistry and morphology of a nanoparticle, remains to be determined. On a related note, further studies of NP–protein interactions may also help understand why nanodiamonds in previous experiments[12,13] did not break the plasma membrane as they broke the endosomal one—a possible factor contributing to this intriguing difference is that their interactions with the former membrane may be primarily mediated by receptor proteins.

Conclusions

Employing continuum modeling of two axial-symmetric nanoparticle models, we examined the energetics of NP-induced membrane pore formation. In summary, such pore formation is found to be energetically favorable when the cost of an open edge is outweighed by wrapping a highly curved part of the NP surface. During this process, membrane adhesion to the rest, less curved parts of the nanoparticle provides the sole driving force. For a rounded cone NP, which mimics the tip of a nanodiamond escaping from an endosome, it must be both sharp ($R \lesssim 4$–5 nm) and large enough ($L \gtrsim 20$ nm) in order to render pore formation energetically favorable. While the latter requirement is estimated numerically, an analytic form is found for the former requirement, providing a quantitative reference for manipulating the NP morphology to break a lipid membrane. Overall, our results agree with the findings of previous experiments and shed light on a general mechanism by which a sharp nanoparticle may spontaneously disrupt the structural integrity of a membrane. For NPs designed to be intracellular biomarkers, biosensors or delivery vessels, such disruption can be exploited as an independent degree of freedom for modulating NP–cell interactions, in order to achieve enhanced endosomal escape and increased cytosolic residence time. Our results have implications in a wide range

of NP-mediated applications, such as cargo delivery, bio-sensing and bio-imaging. Further understanding of the disruptive mode of NP–membrane interactions, which requires more sophisticated treatment of membrane dynamics, should provide additional insight into the design principles of safer and more efficient NP materials.

Conflicts of interest

There are no conflicts to declare.

Acknowledgements

Notes and references

1 C. M. Beddoes, C. P. Case and W. H. Briscoe, *Adv. Colloid Interface Sci.*, 2015, **218**, 48–68.
2 A. E. Nel, L. Mädler, D. Velegol, T. Xia, E. M. V. Hoek, P. Somasundaran, F. Klaessig, V. Castranova and M. Thompson, *Nat. Mater.*, 2009, **8**, 543–557.
3 G. J. Doherty and H. T. McMahon, *Annu. Rev. Biochem.*, 2009, **78**, 857–902.
4 L. I. Selby, C. M. Cortez-Jugo, G. K. Such and A. P. Johnston, *Wiley Interdiscip. Rev.: Nanomed. Nanobiotechnol.*, 2017, **9**, e1452.
5 D. Ma, *Nanoscale*, 2014, **6**, 6415–6425.
6 S. A. Smith, L. I. Selby, A. P. Johnston and G. K. Such, *Bioconjugate Chem.*, 2018, **30**, 263–272.
7 S. Guo and L. Huang, *J. Nanomater.*, 2011, **2011**, 742895.
8 L. Wang, P. Quan, S. H. Chen, W. Bu, Y.-F. Li, X. Wu, J. Wu, L. Zhang, Y. Zhao, X. Jiang, *et al.*, *ACS Nano*, 2019, **13**, 8680–8693.
9 C. M. Goodman, C. D. McCusker, T. Yilmaz and V. M. Rotello, *Bioconjugate Chem.*, 2004, **15**, 897–900.
10 P. R. Leroueil, S. A. Berry, K. Duthie, G. Han, V. M. Rotello, D. Q. McNerny, J. R. Baker, B. G. Orr and M. M. Holl, *Nano Lett.*, 2008, **8**, 420–424.
11 A. M. Sauer, A. Schlossbauer, N. Ruthardt, V. Cauda, T. Bein and C. Braìl̀uchle, *Nano Lett.*, 2010, **10**, 3684–3691.
12 Z. Chu, S. Zhang, B. Zhang, C. Zhang, C.-Y. Fang, I. Rehor, P. Cigler, H.-C. Chang, G. Lin, R. Liu, *et al.*, *Sci. Rep.*, 2014, **4**, 4495.
13 Z. Chu, K. Miu, P. Lung, S. Zhang, S. Zhao, H.-C. Chang, G. Lin and Q. Li, *Sci. Rep.*, 2015, **5**, 11661.
14 Y. Tu, M. Lv, P. Xiu, T. Huynh, M. Zhang, M. Castelli, Z. Liu, Q. Huang, C. Fan, H. Fang and R. Zhou, *Nat. Nanotechnol.*, 2013, **8**, 594–601.

15 R. C. Van Lehn, M. Ricci, P. H. Silva, P. Andreozzi, J. Reguera, K. Voïtchovsky, F. Stellacci and A. Alexander-Katz, *Nat. Commun.*, 2014, **5**, 4482.
16 Z. Ge, Q. Li and Y. Wang, *J. Chem. Theory Comput.*, 2014, **10**, 2751–2758.
17 L. L. Olenick, J. M. Troiano, A. Vartanian, E. S. Melby, A. C. Mensch, L. Zhang, J. Hong, O. Mesele, T. Qiu, J. Bozich, *et al.*, *Chem*, 2018, **4**, 2709–2723.
18 J. Wong-Ekkabut, S. Baoukina, W. Triampo, I.-M. Tang, D. P. Tieleman and L. Monticelli, *Nat. Nanotechnol.*, 2008, **3**, 363.
19 J. Lin, H. Zhang, Z. Chen and Y. Zheng, *ACS Nano*, 2010, **4**, 5421–5429.
20 R. Vácha, F. J. Martinez-Veracoechea and D. Frenkel, *Nano Lett.*, 2011, **11**, 5391–5395.
21 X. Shi, A. von Dem Bussche, R. H. Hurt, A. B. Kane and H. Gao, *Nat. Nanotechnol.*, 2011, **6**, 714–719.
22 J. Lin and A. Alexander-Katz, *ACS Nano*, 2013, **7**, 10799–10808.
23 C. Huang, Y. Zhang, H. Yuan, H. Gao and S. Zhang, *Nano Lett.*, 2013, **13**, 4546–4550.
24 R. M. Bhaskara, S. M. Linker, M. Vögele, J. Köfinger and G. Hummer, *ACS Nano*, 2017, **11**, 1273–1280.
25 K. Yang and Y.-q. Ma, *Nat. Nanotechnol.*, 2010, **5**, 579–583.
26 H.-m. Ding and Y.-q. Ma, *Nanoscale*, 2012, **4**, 1116–1122.
27 Y. Li, X. Li, Z. Li and H. Gao, *Nanoscale*, 2012, **4**, 3768–3775.
28 Y. Li, H. Yuan, A. von dem Bussche, M. Creighton, R. H. Hurt, A. B. Kane and H. Gao, *Proc. Natl. Acad. Sci. U. S. A.*, 2013, **110**, 12295–12300.
29 R. Guo, J. Mao and L.-T. Yan, *ACS Nano*, 2013, **7**, 10646–10653.
30 H. Gao, *J. Mech. Phys. Solids*, 2014, **62**, 312–339.
31 Z. Ge and Y. Wang, *Annu. Rep. Comput. Chem*, Elsevier, 2016, vol. 12, pp. 159–200.
32 I. R. Cooke and M. Deserno, *J. Chem. Phys.*, 2005, **123**, 224710.
33 S. Izvekov and G. A. Voth, *J. Phys. Chem. B*, 2009, **113**, 4443–4455.
34 R. D. Groot and P. B. Warren, *J. Chem. Phys.*, 1997, **107**, 4423–4435.
35 E. Moeendarbary, T. Ng and M. Zangeneh, *Int. J. Appl. Mech.*, 2009, **1**, 737–763.
36 M. Deserno, *Macromol. Rapid Commun.*, 2009, **30**, 752–771.
37 H.-M. Ding and Y. qiang Ma, *Small*, 2015, **11**, 1055–1071.
38 Q. Cui, R. Hernandez, S. E. Mason, T. Frauenheim, J. A. Pedersen and F. Geiger, *J. Phys. Chem. B*, 2016, **120**, 7297–7306.
39 M. Das, U. Dahal, O. Mesele, D. Liang and Q. Cui, *J. Phys. Chem. B*, 2019, **123**, 10547–10561.
40 M. Deserno, *Phys. Rev. E: Stat., Nonlinear, Soft Matter Phys.*, 2004, **69**, 031903.
41 S. Cao, G. Wei and J. Z. Chen, *Phys. Rev. E: Stat., Nonlinear, Soft Matter Phys.*, 2011, **84**, 050901.
42 A. H. Bahrami, *Soft Matter*, 2013, **9**, 8642–8646.
43 S. Dasgupta, T. Auth and G. Gompper, *Soft Matter*, 2013, **9**, 5473–5482.

44 S. Dasgupta, T. Auth and G. Gompper, *Nano Lett.*, 2014, **14**, 687–693.

45 X. Yi, X. Shi and H. Gao, *Nano Lett.*, 2014, **14**, 1049–1055.

46 J. Agudo-Canalejo and R. Lipowsky, *ACS Nano*, 2015, **9**, 3704–3720.

47 A. Takáts-Nyeste and I. Derényi, *Phys. Rev. E: Stat., Nonlinear, Soft Matter Phys.*, 2014, **90**, 052710.

48 C. Contini, M. Schneemilch, S. Gaisford and N. Quirke, *J. Exp. Nanosci.*, 2018, **13**, 62–81.

49 P. B. Canham, *J. Theor. Biol.*, 1970, **26**, 61–81.

50 W. Helfrich, *Z. Naturforsch., C: Biochem., Biophys., Biol., Virol.*, 1973, **28**, 693–703.

51 W. Rawicz, K. Olbrich, T. McIntosh, D. Needham and E. Evans, *Biophys. J.*, 2000, **79**, 328–339.

52 N. Kučerka, S. Tristram-Nagle and J. F. Nagle, *J. Mol. Biol.*, 2006, **208**, 193–202.

53 J. Pan, S. Tristram-Nagle, N. Kučerka and J. F. Nagle, *Biophys. J.*, 2008, **94**, 117–124.

54 M. Hu, J. J. Briguglio and M. Deserno, *Biophys. J.*, 2012, **102**, 1403–1410.

55 I. Derényi, F. Jülicher and J. Prost, *Phys. Rev. Lett.*, 2002, **88**, 238101.

56 C. Morris and U. Homann, *J. Membr. Biol.*, 2001, **179**, 79–102.

57 M. Simunovic and G. A. Voth, *Nat. Commun.*, 2015, **6**, 7219.

58 Z. Shi and T. Baumgart, *Nat. Commun.*, 2015, **6**, 5974.

59 J. Litster, *Phys. Lett. A*, 1975, **53**, 193–194.

60 C. Taupin, M. Dvolaitzky and C. Sauterey, *Biochemistry*, 1975, **14**, 4771–4775.

61 D. V. Zhelev and D. Needham, *Biochim. Biophys. Acta, Biomembr.*, 1993, **1147**, 89–104.

62 S. A. Akimov, P. E. Volynsky, T. R. Galimzyanov, P. I. Kuzmin, K. V. Pavlov and O. V. Batishchev, *Sci. Rep.*, 2017, **7**, 12152.

63 U. Seifert, K. Berndl and R. Lipowsky, *Phys. Rev. A*, 1991, **44**, 1182.

64 R. Capovilla, J. Guven and J. Santiago, *Phys. Rev. E: Stat., Nonlinear, Soft Matter Phys.*, 2002, **66**, 021607.

65 P. Yang and Z.-C. Tu, *Acta Phys. Sin.*, 2016, **65**, 188701.

66 E. Weinan, W. Ren and E. Vanden-Eijnden, *Phys. Rev. B: Condens. Matter Mater. Phys.*, 2002, **66**, 052301.

67 E. Weinan, W. Ren and E. Vanden-Eijnden, *J. Chem. Phys.*, 2007, **126**, 164103.

68 C. L. Ting, D. Appelö and Z.-G. Wang, *Phys. Rev. Lett.*, 2011, **106**, 168101.

69 C. E. Ashley, E. C. Carnes, G. K. Phillips, D. Padilla, P. N. Durfee, P. A. Brown, T. N. Hanna, J. Liu, B. Phillips, M. B. Carter, *et al.*, *Nat. Mater.*, 2011, **10**, 389–397.

70 K. S. Butler, P. N. Durfee, C. Theron, C. E. Ashley, E. C. Carnes and C. J. Brinker, *Small*, 2016, **12**, 2173–2185.

71 Y. Roiter, M. Ornatska, A. R. Rammohan, J. Balakrishnan, D. R. Heine and S. Minko, *Nano Lett.*, 2008, **8**, 941–944.

72 Y. Roiter, M. Ornatska, A. R. Rammohan, J. Balakrishnan, D. R. Heine and S. Minko, *Langmuir*, 2009, **25**, 6287–6299.

73 U. Seifert, *Adv. Phys.*, 1997, **46**, 13–137.

74 E. Evans, V. Heinrich, F. Ludwig and W. Rawicz, *Biophys. J.*, 2003, **85**, 2342–2350.

75 R. Cai and C. Chen, *Adv. Mater.*, 2019, **31**, 1805740.